Scaling laws for high-order-harmonic generation with midinfrared laser pulses

M. V. Frolov,[1,2,3] N. L. Manakov,[1] Wei-Hao Xiong,[4] Liang-You Peng,[3,4,5] J. Burgdörfer,[3,6] and Anthony F. Starace[3,7]

[1]*Department of Physics, Voronezh State University, Voronezh 394006, Russia*

[2]*Institute of Applied Physics, Russian Academy of Sciences, Nizhny Novgorod 603950, Russia*

[3]*Kavli Institute for Theoretical Physics, University of California, Santa Barbara, California 93106-4030, USA*

[4]*Department of Physics, State Key Laboratory for Mesoscopic Physics, Peking University, Beijing 100871, China*

[5]*Collaborative Innovation Center of Quantum Matter, Beijing 100871, China*

[6]*Institute for Theoretical Physics, Vienna University of Technology, Wiedner Hauptstraße 8-10, A-1040 Vienna, Austria, EU*

[7]*Department of Physics and Astronomy, The University of Nebraska, Lincoln, Nebraska 68588-0299, USA*

(Received 16 June 2015; published 10 August 2015)

We derive an analytic expression for the wavelength scaling of the high-order-harmonic generation (HHG) yield induced by midinfrared driving laser fields. It is based on a quasiclassical description of the returning electron wave packet, which is shown to be largely independent of atomic properties. The accuracy of this analytic expression is confirmed by comparison with results of numerical solutions of the time-dependent Schrödinger equation for wavelengths in the range of 1.4 μm $\leq \lambda \leq$ 4 μm. We verify the wavelength scaling of the HHG yield found numerically for midinfrared laser fields in a recent paper by Le *et al.* [Phys. Rev. Lett. **113**, 033001 (2014)].

DOI: 10.1103/PhysRevA.92.023409 PACS number(s): 32.80.Wr, 42.50.Hz, 42.65.Ky, 32.80.Fb

I. INTRODUCTION

Significant progress in the development of intense laser sources having midinfrared (IR) and even far-IR laser wavelengths has stimulated a growing interest in strong-field processes in the deep tunneling regime [1–3]. Since the energetics of this strong-field process is governed by the ponderomotive energy U_p of a tunnel-ionized electron in a laser field (where $U_p \propto \lambda^2$), increasing the laser wavelength λ opens the way for producing higher-energy photons and electrons in strong-field reactions. For high-order-harmonic generation (HHG), such long-wavelength laser sources allow experimentalists to utilize higher-pressure gas targets and to extend phase-matching conditions into the x-ray regime, thus enabling the production of a nearly continuous spectrum of high-order harmonics having extremely short wavelengths [4–9]. As the wavelength increases, these beneficial macroscopic features of the target medium for phase matching compete with the negative feature of the microscopic single-atom HHG yield, which decreases rapidly [1,10]. Therefore, the dependence (or scaling) of the single-atom HHG yield as a function of laser wavelength has become crucially important for the generation of attosecond [4,11] and even, possibly, zeptosecond pulses [12]. Consequently, different schemes for achieving a more favorable λ dependence of the single-atom HHG yield have been suggested [13,14].

The HHG process depends nonlinearly on many parameters. Determining the λ scaling of HHG as a function of any one of these parameters (e.g., laser intensity, ponderomotive energy, harmonic energies, laser pulse duration, etc.) requires that all other parameters remain fixed. Depending on which parameters are kept fixed, different scaling laws can be obtained. Thus, for example, if the laser intensity and the interval of harmonic energies are fixed, the energy radiated per unit time into this interval (an integrated HHG yield) scales as $\lambda^{-\mu}$, where $5 \leqslant \mu \leqslant 6$ [1,10,15–18]. If the ponderomotive energy U_p is kept fixed instead of the intensity, the HHG yield decreases exponentially with λ [19]. In contrast to these two cases, however, if harmonic energies are not fixed, the HHG yield for a fixed intensity may even increase with increasing wavelength λ due to atomic structure effects [20].

Systematic study of the wavelength dependence of the HHG yield began with investigations of the fine-scale oscillations in the λ dependence of integrated harmonic yields [15–18]. These oscillations modulate the smooth λ dependence $\propto \lambda^{-\mu}$ predicted earlier in Ref. [1]. Quasiclassical analyses find that these oscillations originate from the interference of high-order quantum orbits [15,17], whereas a rigorous quantum analysis finds that these oscillations are a manifestation of threshold phenomena in the HHG yield at the closing of multiphoton ionization channels [16,18]. As shown in Ref. [18], the positions of the maxima of these oscillations depend on the shape of the atomic potential: For a short-range potential they coincide with the positions of multiphoton thresholds [16], whereas the corresponding peaks for a Coulomb potential occur in the middle between two neighboring multiphoton thresholds [18]. (Similar features have been found in strong-field ionization of an electron in a Coulomb potential [21]).

Another kind of wavelength scaling for the HHG process has been studied in Refs. [22,23] based on an improved version of the strong-field approximation [24]. Instead of the integrated HHG yield analyzed previously in Refs. [15–18], Refs. [22,23] analyzed the HHG conversion efficiency (CE) for a given harmonic frequency Ω, which is proportional to the HHG yield integrated over the energy interval $[\hbar(\Omega-\omega),\hbar(\Omega+\omega)]$, where $\omega = 2\pi c/\lambda$ is the frequency of the driving field. In the tunneling regime, Refs. [22,23] show that the CE scales as λ^{-5} at the HHG plateau cutoff for a fixed cutoff energy, as λ^{-9} at the cutoff when the cutoff energy is not fixed, and as λ^{-6} over the plateau region for a fixed harmonic energy.

An analysis of the λ dependence of the HHG yield within the framework of the strong-field approximation and quantum orbit theory was reported in Ref. [25]. Within this approach, the partial HHG yield associated with long orbits was found to scale as $\lambda^{-4.1}$ for a fixed absolute harmonic energy, whereas the yield associated with short orbits decreases more rapidly

with increasing wavelength as $\lambda^{-8.5}$. Although these partial λ scalings of the short- and long-trajectory contributions to HHG strongly differ from each other, the overall trend of the decreasing HHG yield with increasing λ for fixed harmonic energy obtained in Ref. [25] agrees with earlier results.

Recently, interest in the λ scaling of the HHG yield has revived within the context of the universality properties of the returning electron wave packet (EWP) in HHG produced by midinfrared laser pulses [26]. Within the quantitative rescattering theory (QRS), which is based on the phenomenological factorization of the HHG yield in terms of the EWP and the field-free photorecombination cross section [27–29] [as confirmed by numerical solutions of the time-dependent Schrödinger equation (TDSE)], several scaling properties have been suggested in Ref. [26] for the EWP considered as a function of the electron energy E, the U_p-scaled energy $\tilde{E} = E/U_p$, and the carrier wavelength λ of the laser pulse:

(i) for fixed E, the EWP and the spectral density of harmonic radiation scale as $\lambda^{-4.2}$;

(ii) for fixed $\tilde{E}$, the EWP scales as $\lambda^{-1.2}$;

(iii) as a function of $\tilde{E}$, the EWP in the long-wavelength limit scales as $\tilde{E}^{1.5}$;

(iv) over the interval $1.5 \lesssim \tilde{E} \lesssim 3.17$, the EWP scales approximately as $e^{1.2\tilde{E}}$.

In this paper, we present an analytic description of the λ dependence of the HHG yield based on an analysis of the (near-) universal properties of the returning EWP [30,31]. Our results confirm the main conclusions concerning the λ scaling of HHG represented in Ref. [26]. In Sec. II we briefly review the relationship between the HHG yield and the spectral distribution of the returning EWP that, upon radiative recombination, controls the spectral distribution of the emitted harmonic radiation. A detailed analysis of the universal scaling properties of the EWP is given in Sec. III. In Sec. IV we compare our analytic results for the EWP with TDSE results for both hydrogen (H) and helium (He) atoms, compare our analytic λ-scaling result for the HHG yield with TDSE results for H, and discuss the validity of QRS results [26] for the λ scaling of both the EWP and the HHG yields. In Sec. V we summarize our results.

II. DEFINITION OF THE HHG YIELD

The scaling of the yield of high-harmonic radiation as a function of the wavelength λ of the driving infrared laser depends on the precise definition of the HHG yield. In accord with Refs. [1,15–18], we analyze the integrated harmonic yield $\Delta\mathcal{Y}$, which is defined as the energy radiated per unit time by the target atom (subjected to a laser pulse of duration $\mathcal{T}$) into a fixed harmonic energy range $[E_1; E_2]$,

$$\Delta\mathcal{Y} = \frac{1}{\mathcal{T}} \int_{E_1}^{E_2} \rho(E_\Omega) dE_\Omega, \tag{1}$$

where $\rho(E_\Omega)$ is the spectral density of the emitted radiation. When the duration of the driving pulses is kept fixed in terms of the number of optical cycles as assumed in the following, $\mathcal{T}$ scales linearly with λ. Consequently, the prefactor $\mathcal{T}^{-1}$ in Eq. (1) introduces one inverse power of λ to the overall scaling of $\Delta\mathcal{Y}$. Note that Ref. [26] states that for $\lambda \geqslant 3$ μm there is a slower decrease in the HHG yield with increasing λ than found for $\lambda \leqslant 2$ μm in earlier investigations [1,15,16,18]. This was shown in Ref. [32] to be due to the use in Ref. [26] of a different definition of the HHG yield from that in Eq. (1). (Specifically, the authors of Ref. [26] considered a nonintegrated HHG yield $\mathcal{Y}$ for a fixed harmonic energy). Using the definition (1) for $\Delta\mathcal{Y}$, the wavelength scaling results of Ref. [26] for the HHG yield agree with previous wavelength scaling results (see Ref. [32] for details).

For the analytic investigation of the scaling, we make use of the approximate factorization of $\rho(E_\Omega)$ [27–29],

$$\rho(E_\Omega) = w(E,F)\sigma^{(r)}(E), \tag{2}$$

in terms of the field-free photorecombination cross section $\sigma^{(r)}$ for an electron with energy E and the spectral distribution of the returning EWP $w(E,F)$ with $E = E_\Omega - I_p$. This factorization is supported by comparison with numerical solutions of the TDSE and represents the key ingredient for the QRS theory. Since $\sigma^{(r)}(E)$ is independent of the parameters characterizing the laser field, the factor $\sigma^{(r)}$ in Eq. (2) does not contribute to the λ scaling. Specifically, for comparison with our numerical TDSE calculations we will employ the cross section for recombination into the ground state of hydrogen,

$$\sigma^{(r)}(E) = 32\pi\alpha^3 \frac{e^{-4q^{-1}\arctan(q)}}{q^2(q^2+1)^2(1-e^{-2\pi/q})}, \tag{3}$$

where $q = pa_0/\hbar$, $\alpha = e^2/(\hbar c)$, and $p = \sqrt{2mE}$.

The remaining λ dependence of $\Delta\mathcal{Y}$ therefore originates exclusively from the EWP, which we analyze in detail in the next section.

III. ANALYTIC LOW-FREQUENCY RESULTS FOR THE EWP AND THE HHG YIELD

Analytical approximations to $w(E,F)$ have been presented in Refs. [30,31]. They are based upon a quantum-mechanical treatment of an exactly solvable model for an electron in both a short-range potential and a strong laser field [33] and form the starting point of the present investigation of the λ scaling for short low-frequency midinfrared pulses. The analytic model results are extended to the case of HHG by neutral atoms, and the accuracy of the extended results is confirmed by comparison with HHG results obtained by a numerical solution of the TDSE.

A. Definition of the phase-averaged EWP

We consider an atom with an ionization potential I_p exposed to an intense linearly polarized laser pulse with electric field $\mathbf{F}(t) = \hat{\mathbf{z}}F(t)$, where $F(t)$ has a peak value F_0, carrier frequency ω or wavelength $\lambda = 2\pi c/\omega$, and duration $\mathcal{T}$. Within the classical three-step scenario for HHG, the EWP can be expressed in terms of a coherent superposition of contributions from returning closed classical orbits j of electrons escaping from and recombining with the atoms as [31]

$$w(E,F) = \sum_{j,k} s_{jk}\sqrt{w_j w_k}\cos(\varphi_j - \varphi_k), \tag{4}$$

where the phase φ_j for the jth closed orbit is a rapidly varying function of the path index j (see Eq. (55) for φ_j in Ref. [31]) and where $s_{j,k} = 1$ for $j = k$. In our analysis of the λ scaling of HHG, we neglect the fine-scale interference features of HHG spectra. Thus, we average Eq. (4) over the phase φ_j, which is equivalent to the substitution $\cos(\varphi_j - \varphi_k) \to \delta_{j,k}$. The phase-averaged EWP is then given by a sum of partial EWPs w_j,

$$\overline{w(E,F)} = \sum_j w_j. \tag{5}$$

The weight w_j with which each classical orbit contributes is given by [20]

$$w_j = \frac{\pi E_\Omega}{2\hbar\omega^2}\mathcal{I}_j\mathcal{W}_j, \tag{6}$$

where $\mathcal{I}_j$ and $\mathcal{W}_j$ are the ionization and propagation factors, respectively.

B. λ scaling of the partial EWPs w_j

Within the single-active-electron approximation, the ionization factor I_j in Eq. (6) can be approximated in terms of the quasiclassical static tunneling ionization rate $\Gamma_{\rm st}$ of an initially bound state $\psi_{\kappa l m_l}(\mathbf{r})$ by [34]

$$\mathcal{I}_j = \frac{4\tilde{\gamma}_j^2\Gamma_{\rm st}(\tilde{F}_j)}{\pi\kappa v_{\rm at}}, \qquad \tilde{\gamma}_j = \frac{\sqrt{2mI_p}\,\omega}{|e|\tilde{F}_j}, \tag{7}$$

$$\Gamma_{\rm st}(\tilde{F}_j) = \frac{I_p}{\hbar}(2l+1)C_{\kappa l}^2\left(\frac{2F_{\rm at}}{\tilde{F}_j}\right)^{2\nu-1} e^{-2F_{\rm at}(\kappa a_0)^3/(3\tilde{F}_j)}, \tag{8}$$

where $\tilde{F}_j = |F(t_i^{(j)})|$, and $v_{\rm at} = e^2/\hbar$ and $F_{\rm at} = m^2e^5/\hbar^4$ are the atomic units of velocity and field strength. The asymptotic behavior of $\psi_{\kappa l m_l}(\mathbf{r})$ for large r underlying Eq. (7) is given by

$$\psi_{\kappa l m_l}(\mathbf{r})|_{\kappa r\gg 1} = C_{\kappa l}\sqrt{\kappa r}\,r^{-1}(\kappa r)^\nu e^{-\kappa r}Y_{l m_l}(\hat{\mathbf{r}}), \tag{9}$$

where $C_{\kappa l}$ is a dimensionless asymptotic coefficient, l is the electron's angular momentum, $\kappa = \sqrt{2mI_p}/\hbar$, $\nu = Z/(\kappa a_0)$, Z is the charge of the atomic core, and $a_0 = \hbar^2/(me^2)$ is the Bohr radius. In what follows, we consider only initial states (9) with $m_l = 0$ since the contributions to the HHG yield from magnetic sublevels with $m_l \neq 0$ are strongly suppressed in the low-frequency limit [35]. The overall λ scaling of the ionization factor (7) is obviously $\mathcal{I}_j \propto \omega^2 \propto \lambda^{-2}$.

The propagation factor $\mathcal{W}_j$ is expressed in terms of the Airy function Ai(x) [31],

$$\mathcal{W}_j = \frac{p}{m}\frac{\mathrm{Ai}^2(\xi_j)}{(v_{\rm at}\Delta t_j)^3\zeta_j^{2/3}}, \qquad \xi_j = \frac{E - E_{\rm max}^{(j)}}{\zeta_j^{1/3}E_{\rm at}}, \tag{10}$$

$$E_{\rm max}^{(j)} = \mathcal{E}_{\rm max}^{\rm cl}\left(t_i^{(j)},t_r^{(j)}\right) - \frac{F\left(t_r^{(j)}\right)}{F\left(t_i^{(j)}\right)}I_p, \tag{11}$$

$$\zeta_j = -\frac{F^2\left(t_r^{(j)}\right)}{2F_{\rm at}^2}\left(1 - \frac{F\left(t_r^{(j)}\right)}{F\left(t_i^{(j)}\right)} + \frac{\dot{F}\left(t_r^{(j)}\right)}{F\left(t_r^{(j)}\right)}\Delta t_j\right), \tag{12}$$

where $\Delta t_j = t_r^{(j)} - t_i^{(j)}$ is the time interval between tunnel ionization and recombination of the jth trajectory and $E_{\rm at} = e^2/a_0$ is the atomic unit of energy. The explicit form (10) of the propagation factor $\mathcal{W}_j$ for the jth orbit was obtained assuming that the kinetic energy E at the instant of recombination $t_r^{(j)}$ is not too far from the maximum energy $E_{\rm max}^{(j)}$ gained in the laser field, where $\max\{E_{\rm max}^{(j)}\}$ determines the cutoff of the harmonic spectrum. The magnitude of $E_{\rm max}^{(j)}$ is controlled by the maximum classical kinetic energy of a free electron (having zero initial velocity at the time $t_i^{(j)}$ and returning to the same spatial point at the time $t_r^{(j)}$) gained in the laser field [31],

$$\mathcal{E}_{\rm max}^{\rm cl}\left(t_i^{(j)},t_r^{(j)}\right) = \frac{e^2}{2mc^2}\left[A\left(t_r^{(j)}\right) - A\left(t_i^{(j)}\right)\right]^2, \tag{13}$$

where $A(t)$ is the vector potential of the laser pulse $F(t) = -\partial A(t)/(c\,\partial t)$. The pair of times $\{t_i^{(j)},t_f^{(j)}\}$ satisfies the coupled system of two classical equations,

$$A\left(t_i^{(j)}\right) - \frac{1}{t_r^{(j)} - t_i^{(j)}}\int_{t_i^{(j)}}^{t_r^{(j)}} A(t)dt = 0, \tag{14a}$$

$$\frac{1}{c}\frac{A\left(t_r^{(j)}\right) - A\left(t_i^{(j)}\right)}{t_r^{(j)} - t_i^{(j)}} + F\left(t_r^{(j)}\right) = 0. \tag{14b}$$

We emphasize that the index j in the present analysis enumerates *all* closed electron trajectories occurring during the laser pulse [i.e., the real solutions of the classical equations (14)], whereas in Ref. [31] only those trajectories were included for which the ionization ($t_i^{(j)}$) and recombination ($t_r^{(j)}$) times occur during neighboring [jth and $(j+1)$th] half-cycles of the laser pulse. For this reason, the latter results are relevant only in the high-energy region of short-pulse HHG spectra.

If the vector potential $A(t)$ depends on the time only through the combination ωt [so that the substitution $t \to \omega^{-1}\tilde{t}$ removes the ω dependence from the time dependence of $A(t)$], then the system of Eqs. (14) shows explicitly that the times $t_i^{(j)}$ and $t_r^{(j)}$ are linear functions of ω^{-1}. Moreover, these times do not depend on the peak value of the laser field. Indeed, converting the system of Eqs. (14) to dimensionless variables by dividing the vector potential by $A_0 = cF_0/\omega$, the electric field by F_0, and the time by ω^{-1}, the resulting dimensionless system depends only on the shape of the laser pulse. In most cases, the vector potential can be well approximated by a function of ωt (excluding, e.g., the case of a chirped pulse). Approximating the time dependence of $A(t)$ by such a function, the λ scaling of the energy $\mathcal{E}_{\rm max}^{\rm cl}$ coincides with that of the ponderomotive energy $U_p = e^2F_0^2/(4m\omega^2) \propto \lambda^2$,

$$\mathcal{E}_{\rm max}^{\rm cl}\left(t_i^{(j)},t_r^{(j)}\right) = \varepsilon_j U_p \propto \lambda^2, \tag{15}$$

where the prefactor ε_j depends neither on the carrier frequency nor on the peak value F_0. Thus, $\mathcal{E}_{\rm max}^{\rm cl}$ increases quadratically with increasing laser wavelength λ. The λ scaling of the propagation factor follows now from the asymptotic expansion of the Airy function in Eq. (10) for large negative arguments,

$$\xi_j = \frac{E - E_{\rm max}^{(j)}}{\zeta_j^{1/3}E_{\rm at}} < -1. \tag{16}$$

Equation (16) implies that the difference between the energy E of the recombining electron, and its maximum value $E_{\rm max}^{(j)}$

is large on the energy scale given by $\sim(F/F_{\rm at})^{2/3}E_{\rm at}$ [see Eq. (12)]. For moderate driving laser field strengths corresponding to intensities $\lesssim 10^{14}$ W/cm^2, Eq. (16) is already satisfied for energy differences as small as a few eV.

Employing the asymptotic expression of the Airy function and averaging it over its rapid oscillations,

$$\mathrm{Ai}^2(-x) \approx \frac{\sin^2\left(\frac{2}{3}x^{3/2}+\frac{\pi}{4}\right)}{\pi\sqrt{x}} \approx \frac{1}{2\pi\sqrt{x}}, \tag{17}$$

the expression (10) can be simplified to

$$\mathcal{W}_j \approx \frac{p\,\omega^3}{2\pi m(v_{\rm at}\Delta\tau_j)^3\zeta_j^{1/2}}\sqrt{\frac{E_{\rm at}}{E_{\rm max}^{(j)}-E}}, \tag{18}$$

where $\Delta\tau_j = \omega(t_r^{(j)}-t_i^{(j)})$ is independent of the carrier frequency ω (since $t_{i,r}^{(j)} \propto \omega^{-1}$). [Note that contributions for which $E_\Omega > (I_p + E_{\rm max}^{(j)})$ are exponentially suppressed.] In the low-frequency limit, $E_{\rm max}^{(j)} \approx \mathcal{E}_{\rm max}^{\rm cl}(t_i^{(j)},t_r^{(j)}) \propto U_p \gg I_p$ so that, using the definition (15), Eq. (18) can be approximated by

$$\mathcal{W}_j \approx \mathcal{C}_j\omega^3\sqrt{\frac{\tilde{E}}{\varepsilon_j-\tilde{E}}}\,\theta(-\xi_j-1), \tag{19}$$

where $\tilde{E} = E/U_p$ is the U_p-scaled return energy and $\mathcal{C}_j = (\pi v_{\rm at}^2\Delta\tau_j^3\sqrt{2\zeta_j})^{-1}$. In Eq. (19) we have multiplied Eq. (18) by a Heaviside cutoff function $\theta(x)$ to restrict nonzero contributions $\mathcal{W}_j$ to values of the arguments of the Airy functions well separated from the region near -1 where the asymptotic expansion (17) breaks down and Eq. (18) becomes singular. In the low-frequency limit $\tilde{E} < \epsilon_j$, $\mathcal{W}_j$ scales as $\mathcal{W}_j \propto \omega^4$ since $\tilde{E} \propto \omega^2$, whereas for fixed $\tilde{E}$ no obvious universal scaling emerges.

Combining now Eqs. (6), (7), and (19) leads to an approximate analytic expression for the weight of the wave packet w_j for the jth trajectory,

$$w_j \approx \theta\left(\varepsilon_j U_p - E - \zeta_j^{1/3}E_{\rm at}\right)\mathcal{D}_j\omega(\tilde{E}+I_p/U_p)\sqrt{\frac{\tilde{E}}{\varepsilon_j-\tilde{E}}}, \tag{20}$$

with

$$\mathcal{D}_j = \frac{\mathcal{C}_j}{2}\left(\frac{F_0}{\tilde{F}_j}\right)^2\frac{\hbar\kappa}{m v_{\rm at}}\Gamma_{\rm st}(\tilde{F}_j). \tag{21}$$

From Eq. (20), two frequency scalings can be obtained for the averaged EWP in the low-frequency limit (cf. Ref. [26]): (i) for a fixed electron energy E and (ii) for a fixed U_p-scaled energy $\tilde{E}$. Since $\tilde{E} \propto \omega^2$, the first case corresponds to the limit $\tilde{E} \ll \varepsilon_j$ for which we can approximate Eq. (20) by

$$w_j \approx \frac{\omega\mathcal{D}_j(E+I_p)\sqrt{E}}{U_p^{3/2}\sqrt{\varepsilon_j}} \propto \omega^4(E+I_p)\sqrt{E}. \tag{22}$$

Consequently, the phase-averaged wave packet (5) scales as

$$\overline{w(E,F)} = \mathcal{D}\omega^4(E+I_p)\sqrt{E} \propto \lambda^{-4}, \tag{23}$$

where the factor,

$$\mathcal{D} = \frac{8m^{3/2}}{|e|^3F_0^3}\sum_j\frac{\mathcal{D}_j}{\sqrt{\varepsilon_j}} \tag{24}$$

depends only on the shape and intensity of the laser pulse but not on λ. Because of the λ independence of the recombination cross section, the same scaling holds for the spectral density of the harmonic radiation in Eq. (2),

$$\rho(E_\Omega) = \mathcal{D}\omega^4(E+I_p)\sqrt{E}\sigma(E) \propto \lambda^{-4}. \tag{25}$$

Considering now the second case, i.e., a fixed $\tilde{E}$, Eq. (20) implies, to leading order, a linear scaling of the weight of the wave packet with ω, $w_j \sim \omega \sim \lambda^{-1}$. Unlike the first case, the prefactor is not universal but depends on the properties of the path distribution,

$$\overline{w(E,F)} = \omega(\tilde{E}+I_p/U_p)\sqrt{\tilde{E}} \times \sum_j\frac{\mathcal{D}_j\,\theta\left(\varepsilon_jU_p-E-\zeta_j^{1/3}E_{\rm at}\right)}{\sqrt{\varepsilon_j-\tilde{E}}}. \tag{26}$$

For large ponderomotive energies compared to the initial binding energy $I_p/U_p \ll 1$, the averaged wave packet (26) scales with the scaled energy $\tilde{E}$, to leading order, as $\overline{w(E,F)} \propto \tilde{E}^{3/2}$.

C. λ scaling of the HHG yield $\Delta\mathcal{Y}$

In accordance with Eqs. (1) and (2), the ω-scaling law for the EWP allows one to predict the wavelength scaling law for the HHG yield. Indeed, according to Eq. (23), the phase-averaged EWP scales as λ^{-4}, whereas $\mathcal{T}^{-1} \propto \lambda^{-1}$ for a fixed number of cycles in a pulse. Thus the analytical scaling law for $\Delta\mathcal{Y}$ is

$$\Delta\mathcal{Y} \propto \lambda^{-5}. \tag{27}$$

In Sec. IV we show that our analytically derived scaling law (27) agrees well with TDSE results for $\lambda \leqslant 4\ \mu$m.

IV. COMPARISONS OF ANALYTIC SCALING LAWS WITH TDSE AND QRS RESULTS

In order to check the accuracy of our approximate analytic results for the EWP and the resulting λ scaling (27) of the harmonic yield $\Delta\mathcal{Y}$, we compare the analytic predictions in Eqs. (23) and (26) for the scaling of the phase-averaged EWP $\overline{w(E,F)}$ with corresponding results from full TDSE calculations for both H and He atoms. For the TDSE calculations of harmonic spectra, we adopt the same method as was used recently to investigate below-threshold harmonic generation [36]. Essentially, the HHG spectrum is evaluated by computing the Fourier transform of the electron's acceleration, which is recorded at each instant during the evolution of the electron wave packet. The details of our numerical solution of the TDSE can be found in Refs. [37–39]. In brief, we expand the wave function $\Psi(\mathbf{r},t)$ in spherical harmonics, and the radial wave functions are discretized using the finite difference method. The wave function $\Psi(\mathbf{r},t)$ is propagated in real time using the split-operator method with a time step of 0.01 a.u. The maximum radial grid point is taken up to 6000 a.u. with a

grid spacing of 0.1 a.u. An absorption function is applied near the end of the radial box to avoid reflections at the box edge. The maximum angular momentum $L_{\max}$ is taken to be 500 in order to obtain converged HHG spectra at even the longest wavelength ($\lambda = 4\ \mu$m) considered in the present paper. All other parameters are carefully chosen to make sure that all results are fully converged.

To compare our analytically derived scaling laws with QRS results [26] discussed in the Introduction, the TDSE was solved for the same laser pulse as in Ref. [26], i.e., for a trapezoidal pulse with a two-cycle flattop of intensity $I = 10^{14}$ W/cm^2 and half-cycle ramps for turn on and turn off. We note that the oscillations of the HHG results were smoothed in Ref. [26] by using Bezier interpolation whereas we present our TDSE results for the actual HHG spectra calculated. The TDSE quantum prediction for the wave packet $w_{QM}(E,F)$ is determined from the numerical result for the harmonic spectral density $\rho(E_\Omega)$ using Eq. (2),

$$w_{QM}(E,F) = \frac{\rho_{QM}(E_\Omega)}{\sigma^{(r)}(E)}. \tag{28}$$

(Note that w_{QM} can alternatively be directly estimated from the quantum phase-space distribution of the returning wave packet [40] without involving the recombination cross section).

In Fig. 1 we compare our U_p-scaled expression (26) for the averaged quasiclassical EWP $\overline{w(E,F)}$ with w_{QM} for both H and He atoms. To remove the linear dependence of the result (26) on the carrier frequency, we normalize the calculated EWPs for different wavelengths by the factor ω and plot them on the $\tilde{E} \equiv E/U_p$ scale. As shown in Fig. 1(a) for the H atom, our averaged EWP analytic result (26) agrees well with the TDSE results, and the shape of the ratio $\overline{w(E,F)}/\omega$ is essentially independent of the carrier wavelength. The dashed-dotted (red) line in Fig. 1(b), also for the H atom, corresponds to the limit (23), whose smooth dependence on the scaled electron energy $\tilde{E}$ contrasts with the spikelike feature $(\epsilon_j - \tilde{E})^{-1/2}$ predicted by Eq. (26) whenever $\tilde{E}$ approaches the maximum value ϵ_j for a given closed orbit j.

In Fig. 1(b), five such threshold energies can be observed for which a spike occurs: $\varepsilon_1 \approx 0.09$, $\varepsilon_2 \approx 0.65$, $\varepsilon_3 \approx 1.54$, $\varepsilon_4 \approx 2.40$, and $\varepsilon_5 \approx 3.17$. (Note that values for the threshold energies ε_3–ε_5 have been reported in Ref. [41], taking into account quantum corrections). These threshold energies are related to the maxima of the return energies (in units of U_p) that the active electron gains by moving in the laser field along the $1 \leqslant j \leqslant 5$ closed classical trajectories. These closed trajectories may be single-return trajectories, which start at the maximum magnitude of the electric field $|F(t_j)|$ of the jth half-cycle of the laser pulse and finish near the end of the next (neighboring) $(j+1)$th half-cycle as well as multiple-return trajectories for which the excursion time is larger than the period $T = 2\pi/\omega$ of the laser pulse. In particular, for the EWP in Fig. 1(b), ε_5 is related to the single-return trajectory on the flattop of the pulse intensity, ε_1 and ε_3 correspond to double-return trajectories, and ε_2 and ε_4 correspond to triple-return trajectories. Note that the spikelike behaviors of the EWP (or the HHG yield) become more pronounced as the laser wavelength increases. They have been observed previously in both numerical and analytical HHG calculations [12,31]. The present analysis shows that between the two

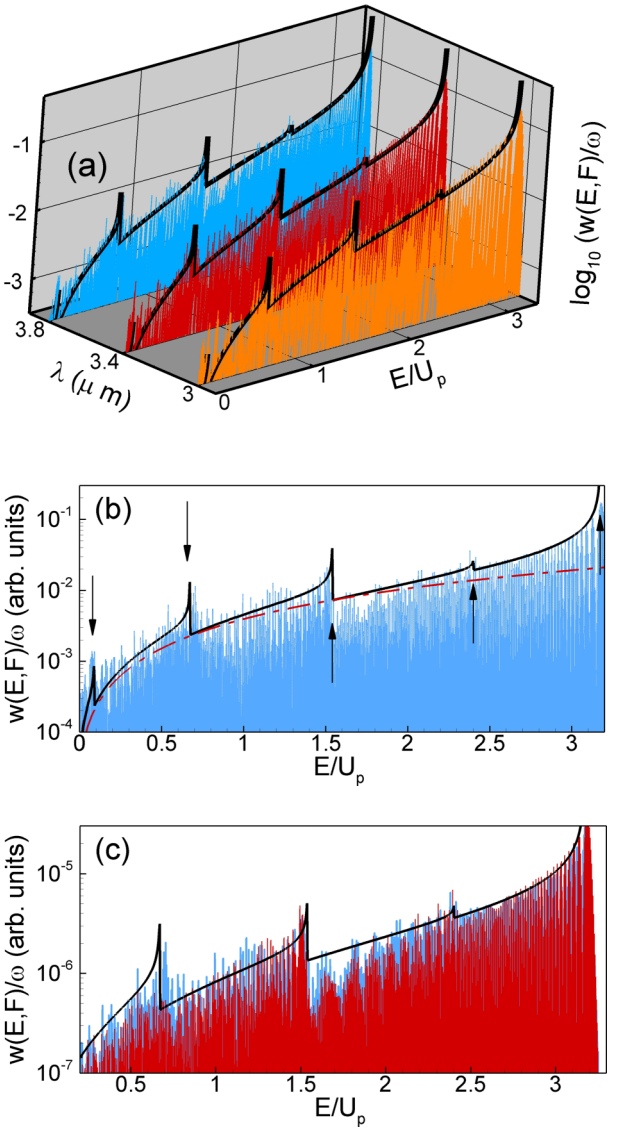

FIG. 1. (Color online) Comparison of different theoretical results for the scaled EWP $\overline{w(E,F)}/\omega$ (arb. units) as a function of the scaled electron energy $\tilde{E} \equiv E/U_p$. (a) Comparison of TDSE results $w_{QM}(E,F)$ for the H atom with the analytic results for three different carrier wavelengths. Filled areas are the TDSE results for $\lambda = 3\ \mu$m (orange filled area), $\lambda = 3.4\ \mu$m (red filled area), and $\lambda = 3.8\ \mu$m (blue filled area) with each for the case of a trapezoidal pulse with a two-cycle flattop of intensity $I = 10^{14}$ W/cm^2 and half-cycle ramps for turn on and turn off. Black lines: analytic results for $\overline{w(E,F)}/\omega$, where $\overline{w(E,F)}$ is given by Eq. (26). (b) For the case of $\lambda = 3.8\ \mu$m, comparison of the TDSE (blue filled area) and analytic results for the H atom using Eq. (26) (black curve with spikes) with the smooth dependence $\propto\sqrt{\tilde{E}}(\tilde{E} + I_p/U_p)$ [cf. Eq. (23)] indicated by the dashed-dotted (red) line. Arrows mark the positions of the threshold energies ε_j, $1 \leqslant j \leqslant 5$ (see text for details). In each case the relative TDSE results are multiplied by a single constant for comparison with the analytic results. (c) Comparison of scaled EWPs $\overline{w(E,F)}/\omega$ for the H and He atoms. Blue filled area: TDSE results for the H atom for a laser field with intensity $I = 10^{14}$ W/cm^2 and $\lambda = 3.8\ \mu$m; red filled area: TDSE results for the He atom for a laser field with intensity $I = 2 \times 10^{14}$ W/cm^2 and $\lambda = 3.2\ \mu$m; black line: analytic result (26) for the EWP calculated for the He atom in a laser field with $I = 2 \times 10^{14}$ W/cm^2 and $\lambda = 3.2\ \mu$m.

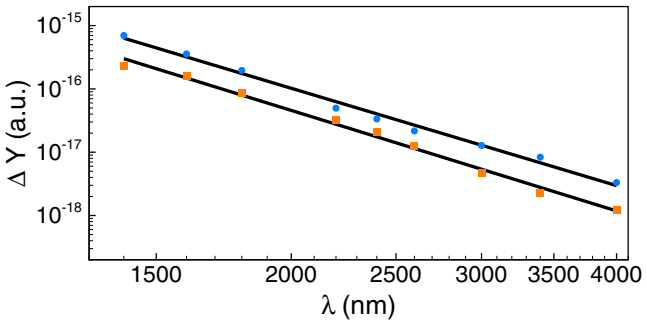

FIG. 2. (Color online) Comparison of TDSE results (symbols) for the HHG yield $\Delta\mathcal{Y}$ defined in Eq. (1) with scaled functions $\propto \lambda^{-\mu}$ (χ^2-fitted solid lines) for two different ranges of the harmonic energies in Eq. (1). Circles: $\Omega \in [20,50]$ (eV), $\mu = 5.1$; squares: $\Omega \in [40,70]$ (eV), $\mu = 5.3$. Results are for the H atom in a two-cycle pulse with $I = 1 \times 10^{14}$ W/cm^2 (as in Ref. [26]).

threshold energies ε_3 and ε_5 (i.e., for $1.5 \lesssim \tilde{E} \lesssim 3.17$), the EWP can be well approximated by

$$\overline{w(E,F)} \propto \frac{\tilde{E}^{1.5}}{\sqrt{\varepsilon_5 - \tilde{E}}}, \tag{29}$$

where we have neglected the correction term I_p/U_p in comparison with $\tilde{E}$ in Eq. (26). The result (29) differs from that in Ref. [26] in which a scaling $e^{1.2\tilde{E}}$ is proposed for this region. We also observe in Fig. 1(b) that the smooth curve [cf. Eq. (23)] representing the limit $\tilde{E} \ll \epsilon_j$ approximates the dependence of the EWP on the scaled energy $\tilde{E}$ quite well with the exception of the regions of spikelike behavior. Since harmonic energies may be of the same order of magnitude as I_p, we have kept the term $\sim I_p\sqrt{E}$ in Eq. (23). Our calculations show that this term can be neglected for $I_p/U_p \ll 10^{-1}$, which corresponds to $\lambda \gg 5$ μm for an intensity of $I = 10^{14}$ W/cm^2 and for hydrogen. [Note that $I_p/U_p \approx 10^{-1}$ for the data in Fig. 1(b).] Thus, the scaling $\overline{w(E,F)}/\omega \propto \tilde{E}^{1.5}$ provides a good approximation only in the deep low-frequency regime for harmonics with energies $E_\Omega \gg I_p$.

In Fig. 1(c) we compare the scaled EWPs for the H and He atoms. The HHG spectrum for He was calculated in the single-active-electron approximation using the potential,

$$V(r) = -\frac{1}{r}\left(1 + \left[1 + \frac{27}{16}r\right]e^{-27/8r}\right). \tag{30}$$

This potential supports a ground s state with binding energy 0.904 a.u., which is close to the recommended value 0.903 a.u. Our comparison shows that, in the long-wavelength limit, the scaled EWP is universal in terms of the scaled energy E/U_p [26].

In Fig. 2 we present TDSE results for the harmonic yield $\Delta\mathcal{Y}$ of the H atom as defined in Eq. (1) for wavelengths up to $\lambda = 4$ μm. The TDSE numerical results show that with increasing λ, $\Delta\mathcal{Y}$ decreases slightly faster than the λ^{-5} behavior predicted by our analytical result (27). Specifically, fits to the TDSE data of a wavelength dependence $\propto \lambda^{-\mu}$ for two ranges of the harmonic energies $\Omega \in [20,50]$ and $\Omega \in [40,70]$ (eV) find that $\mu = 5.1$ and $\mu = 5.3$, respectively, as shown by the two curves in Fig. 2. Possible sources for these minor discrepancies include residual numerical uncertainties in the TDSE calculation, which become increasingly challenging as λ increases. Likewise, the quasiclassical approximation and the restriction to leading terms in the asymptotic expansion underlying our analytic result may contribute to this deviation.

V. SUMMARY

In this paper, we have derived simple analytic expressions [Eqs. (23) and (26)] for the returning EWP in the low-frequency (or long-wavelength) limit that allows one to predict the λ scaling (27) of the harmonic yield. A major simplification in our derivations was achieved by neglecting all interference effects in HHG spectra. Hence, our results for the EWP cannot be used to describe the fine-structure features of HHG spectra. Nevertheless, these analytic formulas for the EWP describe well the shapes of the HHG spectra (averaged over their rapid oscillations) as we have demonstrated in Fig. 1 by their nearly perfect matching with TDSE results for both H and He atoms. Moreover, although the result (26) for the (phase-averaged) EWP does not include interference effects, it remains sensitive to different closed classical electron trajectories, which are responsible for the spikelike behaviors of the HHG spectra as shown in Fig. 1(b). Equation (26) shows explicitly that the shape of the EWP depends on the shape of the laser pulse, which governs the magnitudes of the U_p-scaled threshold energies ε_j. These energies mark the positions of the spikes in the HHG spectra which are related to the maximum energies $\varepsilon_j U_p$ that the active electron can gain by moving along the jth closed trajectory. Neglecting the spikelike features, the EWP can be further simplified and is well represented by Eq. (23). This result for the EWP shows explicitly that, in the deep tunneling regime ($I_p \ll U_p$) and for electron energies in the interval $I_p \ll E \ll 3.17U_p$, the energy scaling of the EWP is given by $E^{1.5}$, independent of the target and the pulse shape. This fact analytically justifies the result of Ref. [26], which was obtained based on numerical analysis of TDSE results. However, our analytic result (26) predicts a dependence of the EWP on $\tilde{E}$ in the interval $1.5 < \tilde{E} < 3.17$ [see Eq. (29)] different from the empirical result $\propto e^{1.2\tilde{E}}$ suggested in Ref. [26].

For fixed absolute values of the electron energy E, the EWP is shown to scale as λ^{-4}. This result is close to the result found numerically in Ref. [26], i.e., $\lambda^{-4.2}$. For a fixed U_p-scaled energy $\tilde{E}$, our results show that the EWP scales as λ^{-1}, which is also close to the result of Ref. [26], i.e., $\lambda^{-1.2}$. Employing these results we have shown both analytically and numerically that the λ-scaling results for the HHG yield found in prior works [1,10,15–18] remain valid also in the midinfrared region as confirmed by the excellent agreement of our analytical results with TDSE calculations of HHG spectra for wavelengths $\lambda \leqslant 4$ μm (see Fig. 2).

ACKNOWLEDGMENTS

The authors thank Professor J. Biegert for fruitful discussions. Four of the authors (M.V.F., L.-Y.P., J.B., and A.F.S.) gratefully acknowledge the hospitality of the Kavli Institute for Theoretical Physics at the University of California in Santa Barbara where part of this work was carried out with

partial research support from the National Science Foundation (NSF) under Grant No. PHY11-25915. Analytic evaluations in this paper were supported, in part, by the Russian Science Foundation through Grant No. 15-12-10033 (M.V.F.). This work was also supported, in part, by RFBR Grant No. 13-02-00420 and the RF Ministry of Education & Science Project No. 1019 (N.L.M.), NSF Grant No. PHY12-08059 (A.F.S.), the National Natural Science Foundation of China (NNSFC) under Grants No. 11322437 and No. 11121091, and the National Basic Research Program of China (973 Program) under Grant No. 2013CB922402 (L.-Y.P.), and SFB-049 NEXTLITE of the FWF, Austria (J.B.).

[1] J. Tate, T. Auguste, H. G. Muller, P. Salières, P. Agostini, and L. F. DiMauro, Scaling of wave-packet dynamics in an intense midinfrared field, Phys. Rev. Lett. **98**, 013901 (2007).

[2] K. D. Schultz, C. I. Blaga, R. Chirla, P. Colosimo, J. Cryan, A. M. March, C. Roedig, E. Sistrunk, J. Tate, J. Wheeler, P. Agostini, and L. F. Dimauro, Strong field physics with long wavelength lasers, J. Mod. Opt. **54**, 1075 (2007).

[3] P. Colosimo, G. Doumy, C. I. Blaga, J. Wheeler, C. Hauri, F. Catoire, J. Tate, R. Chirla, A. M. March, G.G. Paulus, H. G. Muller, P. Agostini, and L. F. DiMauro, Scaling strong-field interactions towards the classical limit, Nat. Phys. **4**, 386 (2008).

[4] V. S. Yakovlev, M. Ivanov, and F. Krausz, Enhanced phase-matching for generation of soft X-ray harmonics and attosecond pulses in atomic gases, Opt. Express **15**, 15351 (2007).

[5] T. Popmintchev, M.-C. Chen, O. Cohen, M. E. Grisham, J. J. Rocca, M. M. Murnane, and H. C. Kapteyn, Extended phase matching of high harmonics driven by mid-infrared light, Opt. Lett. **33**, 2128 (2008).

[6] T. Popmintchev, M.-C. Chen, A. Bahabad, M. Gerrity, P. Sidorenko, O. Cohen, I. P. Christov, M. M. Murnane, and H. C. Kapteyn, Phase matching of high harmonic generation in the soft and hard X-ray regions of the spectrum, Proc. Natl. Acad. Sci. USA **106**, 10516 (2009).

[7] M.-C. Chen, P. Arpin, T. Popmintchev, M. Gerrity, B. Zhang, M. Seaberg, D. Popmintchev, M. M. Murnane, and H. C. Kapteyn, Bright, coherent, ultrafast soft X-ray harmonics spanning the water window from a tabletop light source, Phys. Rev. Lett. **105**, 173901 (2010).

[8] T. Popmintchev, M.-C. Chen, P. Arpin, M. M. Murnane, and H. C. Kapteyn, The attosecond nonlinear optics of bright coherent X-ray generation, Nat. Photonics **4**, 822 (2010).

[9] T. Popmintchev, M.-C. Chen, D. Popmintchev, P. Arpin, S. Brown, S. Ališauskas, G. Andriukaitis, T. Balčiunas, O. D. Mücke, A. Pugzlys, A. Baltuška, B. Shim, S. E. Schrauth, A. Gaeta, C. Hernández-García, L. Plaja, A. Becker, A. Jaron-Becker, M. M. Murnane, and H. C. Kapteyn, Bright coherent ultrahigh harmonics in the kev X-ray regime from mid-infrared femtosecond lasers, Science **336**, 1287 (2012).

[10] A. D. Shiner, C. Trallero-Herrero, N. Kajumba, H.-C. Bandulet, D. Comtois, F. Légaré, M. Giguère, J-C. Kieffer, P. B. Corkum, and D. M. Villeneuve, Wavelength scaling of high harmonic generation efficiency, Phys. Rev. Lett. **103**, 073902 (2009).

[11] F. Krausz and M. Ivanov, Attosecond physics, Rev. Mod. Phys. **81**, 163 (2009).

[12] C. Hernández-García, J. A. Pérez-Hernández, T. Popmintchev, M. M. Murnane, H. C. Kapteyn, A. Jaron-Becker, A. Becker, and L. Plaja, Zeptosecond high harmonic keV X-ray waveforms driven by midinfrared laser pulses, Phys. Rev. Lett. **111**, 033002 (2013).

[13] K. L. Ishikawa, E. J. Takahashi, and K. Midorikawa, Wavelength dependence of high-order harmonic generation with independently controlled ionization and ponderomotive energy, Phys. Rev. A **80**, 011807(R) (2009).

[14] H. Du, S. Xue, H. Wang, Y. Wen, and B. Hu, Wavelength scaling of high-order harmonic yield from a Rydberg atom in a few-cycle pulse, J. Opt. Soc. Am. B **31**, 1621 (2014).

[15] K. Schiessl, K. L. Ishikawa, E. Persson, and J. Burgdörfer, Quantum path interference in the wavelength dependence of high-harmonic generation, Phys. Rev. Lett. **99**, 253903 (2007).

[16] M. V. Frolov, N. L. Manakov, and A. F. Starace, Wavelength scaling of high-harmonic yield: Threshold phenomena and bound state symmetry dependence, Phys. Rev. Lett. **100**, 173001 (2008).

[17] K. Schiessl, K. L. Ishikawa, E. Persson, and J. Burgdörfer, Wavelength dependence of high-harmonic generation from ultrashort pulses, J. Mod. Opt. **55**, 2617 (2008).

[18] K. L. Ishikawa, K. Schiessl, E. Persson, and J. Burgdörfer, Fine-scale oscillations in the wavelength and intensity dependence of high-order harmonic generation: Connection with channel closings, Phys. Rev. A **79**, 033411 (2009).

[19] T. Auguste, F. Catoire, P. Agostini, L. F. DiMauro, C. C. Chirila, V. S. Yakovlev, and P. Salières, Driving-frequency scaling of high-harmonic quantum paths, New J. Phys. **14**, 103014 (2012).

[20] M. V. Frolov, N. L. Manakov, T. S. Sarantseva, M. Yu. Emelin, M. Yu. Ryabikin, and A. F. Starace, Analytic description of the high-energy plateau in harmonic generation by atoms: Can the harmonic power increase with increasing laser wavelengths?, Phys. Rev. Lett. **102**, 243901 (2009).

[21] K. Krajewska, I. I. Fabrikant, and A. F. Starace, Threshold effects in strong-field ionization: Energy shifts and Rydberg structures, Phys. Rev. A **86**, 053410 (2012).

[22] E. L. Falcão-Filho, V. M. Gkortsas, A. Gordon, and F. X. Kärtner, Analytic scaling analysis of high harmonic generation conversion efficiency, Opt. Express **17**, 11217 (2009).

[23] V.-M. Gkortsas, S. Bhardwaj, E. L. Falcão-Filho, K.-H. Hong, A. Gordon, and F. X. Kärtner, Scaling of high harmonic generation conversion efficiency, J. Phys. B **44**, 045601 (2011).

[24] A. Gordon and F. X. Kärtner, Quantitative modeling of single atom high harmonic generation, Phys. Rev. Lett. **95**, 223901 (2005).

[25] D. R. Austin and J. Biegert, Strong-field approximation for the wavelength scaling of high-harmonic generation, Phys. Rev. A **86**, 023813 (2012).

[26] A.-T. Le, H. Wei, C. Jin, V. N. Tuoc, T. Morishita, and C. D. Lin, Universality of returning electron wave packet in high-order harmonic generation with midinfrared laser pulses, Phys. Rev. Lett. **113**, 033001 (2014).

[27] T. Morishita, A.-T. Le, Z. Chen, and C. D. Lin, Accurate retrieval of structural information from laser-induced photoelectron and

high-order harmonic spectra by few-cycle laser pulses, Phys. Rev. Lett. **100**, 013903 (2008).

[28] A.-T. Le, T. Morishita, and C. D. Lin, Extraction of the species-dependent dipole amplitude and phase from high-order harmonic spectra in rare-gas atoms, Phys. Rev. A **78**, 023814 (2008).

[29] C. D. Lin, A.-T. Le, Z. Chen, T. Morishita, and R. Lucchese, Strong-field rescattering physics–self-imaging of a molecule by its own electrons, J. Phys. B **43**, 122001 (2010).

[30] M. V. Frolov, N. L. Manakov, A. A. Silaev, N. V. Vvedenskii, and A. F. Starace, High-order harmonic generation by atoms in a few-cycle laser pulse: Carrier-envelope phase and many-electron effects, Phys. Rev. A **83**, 021405(R) (2011).

[31] M. V. Frolov, N. L. Manakov, A. M. Popov, O. V. Tikhonova, E. A. Volkova, A. A. Silaev, N. V. Vvedenskii, and A. F. Starace, Analytic theory of high-order harmonic generation by an intense few-cycle laser pulse, Phys. Rev. A **85**, 033416 (2012).

[32] M. V. Frolov, N. L. Manakov, W.-H. Xiong, L.-Y. Peng, J. Burgdörfer, and A. F. Starace, Comment on 'Universality of returning electron wave packet in high-order harmonic generation with midinfrared laser pulses', Phys. Rev. Lett. **114**, 069301 (2015).

[33] M. V. Frolov, N. L. Manakov, and A. F. Starace, Effective-range theory for an electron in a short-range potential and a laser field, Phys. Rev. A **78**, 063418 (2008).

[34] B. M. Smirnov and M. I. Chibisov, The breaking up of atomic particles by an electric field and by electron collisions, Zh. Eksp. Teor. Fiz. **49**, 841 (1965) [Sov. Phys. JETP **22**, 585 (1966)].

[35] M. V. Frolov, A. V. Flegel, N. L. Manakov, and A. F. Starace, Description of harmonic generation in terms of the complex quasienergy. II. Application to time-dependent effective range theory, Phys. Rev. A **75**, 063408 (2007).

[36] W.-H. Xiong, J.-W. Geng, J.-Y. Tang, L.-Y. Peng, and Q. Gong, Mechanisms of below-threshold harmonic generation in atoms, Phys. Rev. Lett. **112**, 233001 (2014).

[37] L.-Y. Peng and A. F. Starace, Application of coulomb wave function discrete variable representation to atomic systems in strong laser fields, J. Chem. Phys. **125**, 154311 (2006).

[38] L.-Y. Peng, E. A. Pronin, and A. F. Starace, Attosecond pulse carrier-envelope phase effects on ionized electron momentum and energy distributions: Roles of frequency, intensity and an additional IR pulse, New J. Phys. **10**, 025030 (2008).

[39] M.-H. Xu, L.-Y. Peng, Z. Zhang, Q. Gong, X.-M. Tong, E. A. Pronin, and A. F. Starace, Attosecond streaking in the low-energy region as a probe of rescattering, Phys. Rev. Lett. **107**, 183001 (2011).

[40] S. Gräfe, J. Doose, and J. Burgdörfer, Quantum phase-space analysis of electronic rescattering dynamics in intense few-cycle laser fields, J. Phys. B **45**, 055002 (2012).

[41] D. B. Milošević and W. Becker, Role of long quantum orbits in high-order harmonic generation, Phys. Rev. A **66**, 063417 (2002).